

# RSC Advances



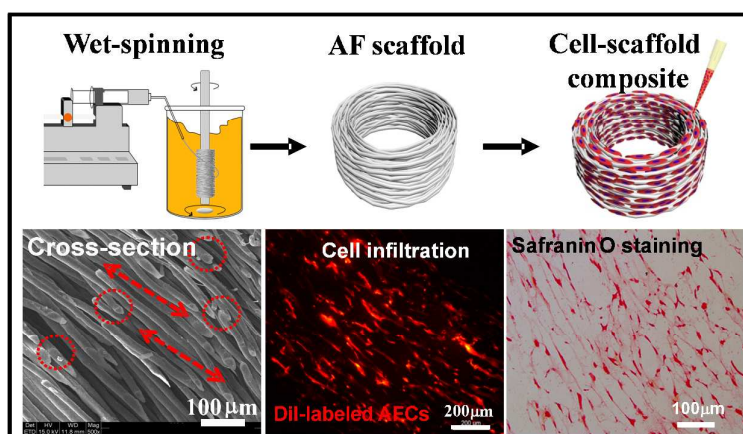
This is an *Accepted Manuscript*, which has been through the Royal Society of Chemistry peer review process and has been accepted for publication.

*Accepted Manuscripts* are published online shortly after acceptance, before technical editing, formatting and proof reading. Using this free service, authors can make their results available to the community, in citable form, before we publish the edited article. This *Accepted Manuscript* will be replaced by the edited, formatted and paginated article as soon as this is available.

You can find more information about *Accepted Manuscripts* in the [Information for Authors](#).

Please note that technical editing may introduce minor changes to the text and/or graphics, which may alter content. The journal's standard [Terms & Conditions](#) and the [Ethical guidelines](#) still apply. In no event shall the Royal Society of Chemistry be held responsible for any errors or omissions in this *Accepted Manuscript* or any consequences arising from the use of any information it contains.

## Graphical Abstract



**Circumferentially Oriented Microfiber Scaffold Prepared by Wet-spinning for  
Tissue Engineering of Annulus Fibrosus**

Baoshan Xu,<sup>1,3,†</sup> Lilong Du,<sup>1,3,†</sup> Jiamin Zhang,<sup>2</sup> Meifeng Zhu,<sup>2</sup> Shenglu Ji,<sup>2</sup> Yang  
Zhang,<sup>1</sup> Deling Kong,<sup>2</sup> Xinlong Ma,<sup>1</sup> Qiang Yang<sup>1\*</sup> and Lianyong Wang<sup>2\*</sup>

<sup>1</sup>Department of Spine Surgery, Tianjin Hospital, Tianjin 300211, People's Republic  
of China

<sup>2</sup>Key Laboratory of Bioactive Materials, Ministry of Education, College of Life  
Sciences, Nankai University, Tianjin 300071, People's Republic of China

<sup>3</sup>Tianjin Medical University, Tianjin 300070, People's Republic of China

<sup>†</sup>These authors contributed equally to this work

**Corresponding authors:**

\* **Lianyong Wang**, E-mail: [wly@nankai.edu.cn](mailto:wly@nankai.edu.cn)

\* **Qiang Yang**, E-mail: [yangqiang1980@126.com](mailto:yangqiang1980@126.com)

**ABSTRACT:** Repairing damaged annulus fibrosus (AF) is one of the most challenging topics for treating intervertebral disc (IVD) disease. Tissue engineering combining scaffolds with cells provides a promising solution. However, fabricating scaffolds with circumferentially oriented fibrous structure similar to native AF remains a big challenge. In this study, we present an effective and convenient wet spinning strategy for fabricating AF scaffold composed of circumferentially oriented poly ( $\epsilon$ -caprolactone) microfibers. Cell culture experiments demonstrated that this scaffold could support AF cell attachment, proliferation and infiltration as confirmed by scanning electron microscopy (SEM), confocal microscopy, live/dead staining and MTT assay, respectively. Histological, immunohistochemical staining, biochemical quantitative analysis and RT-PCR showed that the AF cells (AFCs) inside scaffolds could spread along the microfiber direction and secrete AF-related extracellular matrix (*e.g.*, glycosaminoglycans, collagen type I and II) which also oriented along the microfiber direction. As a result, the compressive and tensile properties were enhanced with increasing culture time. These results demonstrate the feasibility of using this new wet-spun microfibrillar oriented scaffold for AFCs culture, and the potential application for regeneration of AF.

**KEYWORDS:** annulus fibrosus; wet-spinning; AF extracellular matrix; fibrous scaffold; poly ( $\epsilon$ -caprolactone).

## 1. Introduction

Intervertebral disc (IVD) is a complex connective tissue lying between adjacent vertebrae responsible for both load transmission and spine mobility,<sup>1,2</sup> which consists of inner nucleus pulposus (NP) and outer annulus fibrosus (AF).<sup>3</sup> IVD degeneration, characterized by progressive microstructural disorder of the AF as well as dehydration and fibrosis of the NP, is considered as a major source of lower back pain and limited spine mobility.<sup>4,5</sup> Although there exist several treatments for severe IVD degeneration (e.g., discectomy, spinal fusion and total disc replacement), they are associated with several side effects such as recurrent disc herniation, limited mobility and degenerative changes in adjacent vertebrae.<sup>6,7</sup> Therefore, new and more effective methods for treating IVD degeneration are urgently needed.<sup>8-11</sup> Cell-based tissue engineering provides a promising solution for treating severe IVD degeneration by combining biomaterial and appropriate cells,<sup>12,13</sup> where regeneration of functional AF is one of the most challenging topics.

Native AF is multi-lamellar structure consisting of 15 to 25 concentric layers of collagen fibers. This organization and composition of AF confers biomechanical function to the spine.<sup>14,15</sup> Thus, an ideal scaffold for AF tissue engineering should have the shape, structure and mechanical properties similar to that of natural AF. To this end, various aligned fibrous scaffolds have been developed for AF tissue engineering, such as toroidal silk scaffold with a lamellar structure fabricated by using freeze-drying.<sup>16</sup> However, the lamellar structures generated were not circumferentially oriented. Electrospinning methods has been explored to fabricate AF scaffold with nanoscale fiber which can guide the seeded cells to orientate and deposit the extracellular matrix (ECM) along the direction of the fiber.<sup>17-22</sup> However, A obvious disadvantage of electrospun nanofiber scaffolds is that it is very difficult for cells to infiltrate throughout this scaffolds because of the small pore size resulting from tightly packed nanofibers.<sup>23,24</sup> To address this limitation, a multi-lamellar architecture was fabricated by wrapping the stacked electrospun sheets onto which the cells were seeded. However, the lack of stability of the 3D structure and weak compressive strength hindered its applications.<sup>25</sup> Compared to electrospinning, the wet-spinning is a more straightforward and safe method used for fabricating fibrous scaffolds with

microscale fibers. In wet-spinning process, the polymeric solution is extruded into a coagulation bath to precipitate the polymer in the form of a fiber because of solvent diffusion. The polymer fibers could be collected onto collectors to create fibrous scaffolds.<sup>26,27</sup> Wet-spun microfibers have attracted considerable interest as a scaffold matrix to guide and direct the behavior of cells for a variety of applications, such as cartilage, tendon and ligament tissue engineering.<sup>28,29</sup> However, there are few concerns about the application of wet-spinning to fabrication of AF scaffolds.

PCL is a non-toxic, good biocompatibility and highly elastic polyester biomaterial that possesses a slow degradation of 1-2 years in vivo. PCL has been approved by FDA to be used in the fields of biomedicine including tissue engineering scaffold and drug delivery system.<sup>30</sup> In the current study, we successfully fabricated a 3D PCL scaffold with circumferentially oriented microfibers by wet-spinning. AF cells (AFCs) were seeded onto this scaffold to evaluate the feasibility of constructing tissue-engineered AF.

## **2 Materials and methods**

### ***2.1 Fabrication of oriented micro-fibrous scaffolds***

The oriented poly ( $\epsilon$ -caprolactone) (PCL) microfiber scaffold was fabricated by a wet-spinning process as shown in Fig. 1. In this new wet-spinning system, we used a blended solution of edible oil and hexane as coagulation bath in which the viscous edible oil could produce adequate shear force to deform spin dope to develop into micro-sized fibers. We dissolved PCL pellets in  $\text{CHCl}_3/\text{THF}$  (3:1, v/v) to prepare the homogenous spinning solution with a matched specific gravity relative to coagulation bath so that most microfibers could be wrapped onto rotating mandrel. Detailly, the homogenous PCL solution was poured into a 10-mL glass syringe equipped with a 5# gauge blunt-tipped needle, which was submerged into a coagulation bath using a syringe pump, the spin dope of PCL solution was extruded into the coagulation bath at a certain flow rate. The spin dope was deformed and finally developed into micro-sized fibers by the shear force generated by a rotating magnetic stirrer. The micro-sized fibers were collected by wrapping them around a 3-mm-diameter stainless-steel mandrel rotating. After desired volume of PCL solution was extruded, the collected microfibers were removed from the mandrel, washed in excess hexane to remove oil and dried in a vacuum desiccator for 2 days to remove residual reagents.

This process produced a circular structure comprised of PCL microfibers and used as the AF scaffold.

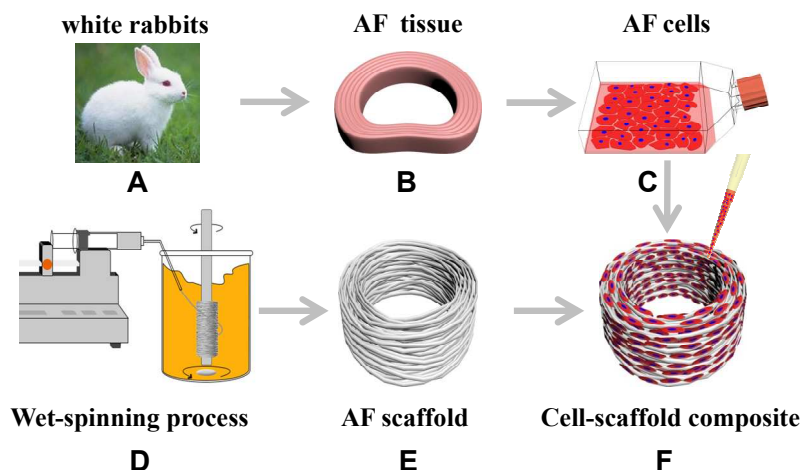


**Fig. 1** Schematic illustration of fabrication of scaffold and AFCs-scaffold composite. AF tissues (B) were separated from New Zealand white rabbits (A), followed by digesting to obtain the primary AFCs (C). Oriented micro-fibrous 3D scaffolds with 6 mm outer diameter, 3 mm inner diameter and 2 mm thickness (E) were obtained by cutting the wet-spun samples (D). AFCs-scaffold composite was formed by seeding AFCs onto AF scaffold (F).

## 2.2 Scaffold characterization

The morphologic features of scaffolds (both cross- and longitudinal sections) were examined by scanning electron microscopy (SEM, Hitachi X-650, Japan) after sputter-coating with gold. The microfiber diameters were determined by measuring at least 50 fibers from SEM images by use of Image J (US National Institutes of Health). Porosity was measured by a weighing method.<sup>31</sup>

## 2.3 Isolation and culture of AFCs

AFCs were isolated from spines of 4-week-old New Zealand white rabbits following the protocols from literature.<sup>17</sup> Animal surgery protocols were approved by the Animal Experimental Ethics Committee of Tianjin Hospital. Briefly, spines were dissected, the muscle and ligament tissues surrounding IVDs were then removed. The IVDs from T10 to L5 were sectioned transversely and AF tissues were separated by use of a scalpel blade. The AF tissues were minced and digested in 0.2% (w/v) collagenase type II (Sigma–Aldrich) for 3 to 4 h at 37°C, filtered through a nylon mesh and centrifuged at 1200 rpm for 5 min to harvest primary AFCs, then resuspended and

cultured in Dulbecco's modified Eagle's medium (DMEM) containing 1% antibiotics and 10% fetal bovine serum (Gibco). Second-passage AFCs were used for next experiments.

#### **2.4 Cell seeding**

PCL micro-fibrous scaffolds (6mm outer diameter, 3 mm inner diameter and 2 mm thickness) were sterilized by  $^{60}\text{Co}$   $\gamma$  irradiation, then soaked in DMEM overnight before cell seeding. 40  $\mu\text{L}$  cell suspension of second passage AFCs ( $1 \times 10^7$  cells/mL) was uniformly seeded onto scaffolds. The cell-seeded scaffolds were placed in a 24-well culture plate and incubated for 3 h before the addition of 1 mL culture medium into the well. The cell-seeded scaffolds were continuously cultured for predetermined days and the culture medium was changed every day.

#### **2.5 Cell behavior on scaffolds**

**Cell attachment and spread.** Cell-scaffold composites cultured for 3, 7 and 14 days were fixed overnight with 2.5% glutaraldehyde, dehydrated in a graded series of ethanol, dried and coated with gold. Then the cell attachment and spread onto the scaffolds was observed by SEM.

**Cell cytoskeleton organization.** For observing cell cytoskeleton organization, the cell-scaffold composites were fixed with 4% formaldehyde after culture for 7 and 14 days, washed with phosphate buffered saline (PBS), then permeabilized with 0.1% Triton X-100 for 5 min. After washing with PBS, cell-scaffold specimens were incubated with rhodamine-phalloidin (Sigma-Aldrich) for 60 min at room temperature, washed with PBS and counter-stained with DAPI for 10 min, then the cell cytoskeleton organization was viewed by laser confocal microscopy (Leica, Germany).

**Cell infiltration.** To evaluate cell infiltration inside scaffolds *in vitro*, AFCs were labeled with DiI (1,1'-dioctadecyl-3,3',3'-tetramethylindocarbocyanine perchlorate) before seeding. Cell-scaffold composites cultured for 7 and 14 days were harvested, fixed in 4% formaldehyde overnight, dehydrated in 30% sucrose for 24 h, then embedded in OCT compound. We obtained 6- $\mu\text{m}$ -thick cross- and longitudinal sections by use of a Leica cryomicrotome (Leica, Wetzlar, Germany). Fluorescent images of sections were obtained by stereomicroscopy (DMI 4000, Leica, Germany).

**Cell viability.** Cell viability in scaffolds was assessed by using live/dead kit (Invitrogen). Cell-scaffold composites cultured for 14 days were gently rinsed twice with PBS, then incubated with the live/dead staining solution at 37 °C for 30 min.

Live cells (green) and dead cells (red) were observed by laser confocal microscopy. (Leica, Germany).

**Metabolic activity.** The metabolic activity of AFCs in the scaffolds was evaluated by MTT assay. Cell-scaffold composites were cultured for 1, 7 and 21 days, then the culture medium was removed, and 50  $\mu$ L MTT (3-(4,5-dimethylthiazol-2-yl)-2,5-diphenyltetrazolium bromide) solution (5 mg/mL) was added to each well for incubation at 37 °C for 4 h. The MTT solution was removed and replaced with 800  $\mu$ L DMSO for continuous shaking in the dark. 100  $\mu$ L supernatant was transferred to 96-well plates, and the optical density (OD) at 490 nm was measured by use of a microplate reader (iMark, Bio RAD, Japan).

**2.6 Histological and immunohistochemical staining.** For histological staining, AF cell-scaffold samples were fixed with 4% formaldehyde, dehydrated, paraffin-embedded and cut into sections 6  $\mu$ m thick by use of a microtome (RM2016, Leica, Germany). The sections were stained with hematoxylin and eosin (H&E), and imaged by inverted light microscopy (Ix53, Olympus, Japan). For observation of GAGs, the sections were stained with Safranin-O (Sigma–Aldrich). Immunohistochemical staining was used to examine collagen type I and type II by the following procedure: the deparaffinized sections were treated with 3% H<sub>2</sub>O<sub>2</sub> solution for 30 min, incubated with 5% bovine serum albumin (BSA) for 30 min at 37 °C, then primary antibody (rabbit anti-collagen I and II, Bioss, China) overnight at 4 °C, washed and incubated with biotinylated secondary antibodies (Santa Cruz Biotechnology). Treated sections were developed with diaminobenzidine (DAB) (Vector Laboratories, CA) and observed by inverted microscopy (Leica, Germany).

**2.7 Quantitative assays for DNA, GAGs and collagen.** Quantitative analysis of DNA, GAGs and collagen was performed for AF cell-scaffold samples cultured for 1, 7, and 21 days. The DNA content could be used to study cell proliferation because the DNA content was assumed to be proportional to cell number. We determined by the Hoechst 33258 dye binding assay (Sigma–Aldrich).<sup>32</sup> Total GAG content was quantified by the 1,9-dimethylmethylene blue (DMMB) dye-binding assay with a commercially available kit (Genmed Scientifics Inc, USA).<sup>33</sup> Collagen type I and II content was quantified by ELISA kits (R&D Systems, USA) (Blue Gene).<sup>34</sup> All results were normalized to dry weight of scaffold.

### 2.8 Real-time PCR.

AF cell-scaffold samples were cultured for 1, 7 and 21 days, then cell-scaffold composites ( $n=3$ ) were rinsed with PBS, cut into small pieces, disrupted, and lysed with 1.0 mL TRIzol reagent (Invitrogen, Carlsbad, CA, USA). Total RNA was extracted by use of the RNeasy kit (Invitrogen, USA). Total RNA concentration was quantified by spectrophotometry (NanoDrop1000, USA) at 260 nm wavelength. Subsequently, 2  $\mu$ g of RNA was reverse-transcribed into cDNA with use of reverse transcriptase premix (Promega, WI, USA). The expression of collagen type Ia1 (*Col Ia1*), collagen type IIa1 (*Col IIa1*), and *aggrecan* was quantified by a real-time PCR system (Applied Biosystems, USA) with the SYBR Green system (Fermentas Life Sciences) at 94 $^{\circ}$ C for 4 min, followed by 40 cycles at 94 $^{\circ}$ C for 30 s, 56 $^{\circ}$ C for 60 s and 72 $^{\circ}$ C for 40 s. Relative expression of target genes was normalized by the Ct value of housekeeping gene of  $\beta$ -actin with the  $2^{-\Delta\Delta C_t}$  method. The primer sequences for *aggrecan*, *Col Ia1*, *Col IIa1* and  *$\beta$ -actin* are listed in Table 1.

### 2.9 Mechanical testing.

The tensile and compressive moduli of scaffold were determined by a micro-material mechanical testing system (MTF-100, China). Samples were immersed in PBS for at least 4 h before tests. The AF cell-scaffold composites ( $n=3$ ) were compressed at a constant rate of 1 mm/min. Compressive modulus was determined from the slope of the ascending linear region of the stress-strain curve. Before testing tensile properties, the blank and cell-seeded scaffolds were dissected into rectangular samples of 10  $\times$  2  $\times$  0.5 mm (length  $\times$  height  $\times$  width), then pulled at a rate of 10 mm/min. Tensile modulus (Young's modulus) was calculated as the slope of the linear portion of the stress-strain curve.

### 2.10 Statistical analysis.

All quantitative experiments data were obtained from at least three samples and reported as mean  $\pm$  SD. Statistical analysis of data involved one-way ANOVA. A multiple comparison test (Tukey's method) was performed if the difference was significant. Differences between groups were considered statistically significant at  $p<0.05$ .

## 3. Results and discussion

In this study, we have successfully fabricated a 3D PCL scaffold with circumferentially oriented microfibers by wet-spinning. This kind of wet-spun AF scaffold had three superior advantages, *i.e.*, mimicking the circumferentially oriented

structure of the native AF, supporting AFCs penetration throughout the interior of scaffolds, and guiding oriented growth of AFCs and oriented deposition of AF-related ECMs.

### 3.1 Fabrication and characterization of scaffolds

To optimize the wet spinning process parameters, we investigated the effects of three main factors (i.e. polymer concentration, flow rate of PCL solution, rotating speed of the mandrel) on the morphology and diameter of fabricated fibers. The results showed that the concentration of PCL solution has large influence on fiber diameter and morphology (Fig. 2A-C). With the increase of concentration from 2 to 15%, the microfiber changed from irregular shape to smooth and regular shape, with microfiber diameter increasing from  $4.90\pm 1.62$  to  $21.78\pm 2.47$   $\mu\text{m}$  (Fig. 2D). Under the condition of 10% PCL solution and 600 rpm of rotation speed, the increase of flow rate from 1 to 8 mL/h did not produce apparent change in microfibers morphology (Fig. 3). Otherwise, the microfiber diameter increased from  $15.31\pm 2.31$  to  $27.39\pm 4.37$   $\mu\text{m}$  ( $p<0.01$ ) (Fig. 3D).

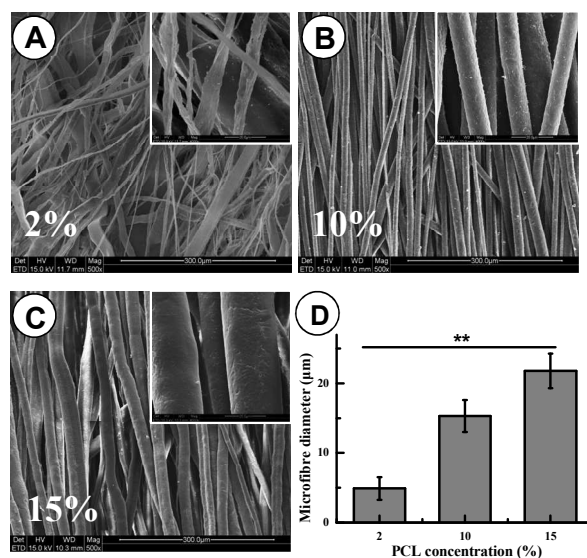


**Fig. 2** Effects of PCL concentration on diameter and morphology of fibers under flow rate 1mL/h and rotating speed 600 rpm. Scanning electron microscopy (SEM) images of the fibers prepared at three concentrations (A) 2%, (B) 10% and (C) 15%, corresponding insets are high-magnification images of the fibers. (D) Changes of microfiber diameters.

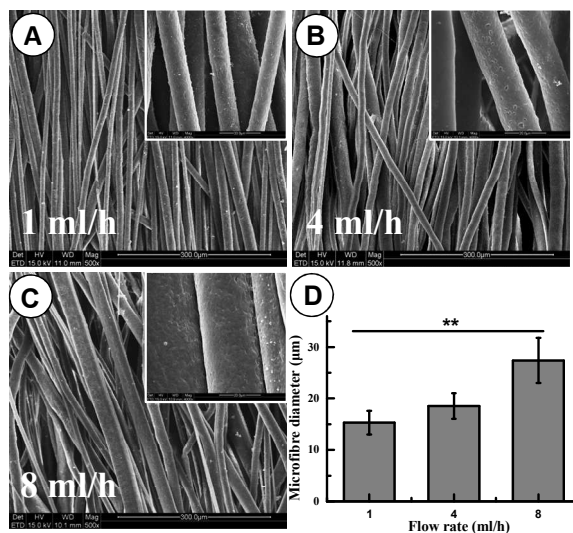


**Fig. 3** Effects of flow rate on diameter and morphology of fibers under PCL concentrations 10% and rotation speed 600 rpm. Scanning electron microscopy (SEM) images of the fibers prepared at three flow rate (A) 1mL/h, (B) 4mL/h and (C) 8mL/h, corresponding insets are high-magnification images of the fibers. (D) Changes of microfiber diameters.

On the basis of above results, we fabricated 3D scaffolds using the rotating speed of 300, 600 and 1000 rpm under flow rate 1mL/h and concentration 10%. We found that the three fabricated 3D scaffolds appeared in the as-desired annulus shape and contained concentric oriented PCL fibers (Fig. 4A-C). The quantified fiber diameters varied from  $22.96 \pm 4.48$  to  $11.62 \pm 3.21 \mu\text{m}$  when rotating speed changed from 300 to 1000 rpm (Table 2). Most fibers in the scaffold ran parallel to each other, while a few fibers crossed with certain angle inside S3 and S6. When rotating speed increased to 1000 rpm, the microfibers were fused to each other resulting in a more compact scaffold (Fig. 4C1-C2). Consequently, the porosity of scaffolds sharply decreased to  $42.58 \pm 4.39\%$  from  $81.24 \pm 8.75\%$  of S3 (Table 2). These changes could be explained as follows. In our developed wet-spinning system, when the droplets of PCL solution were extruded into the coagulation bath, the shear forces will draw the droplets to form liquid polymer streams, which were further transformed into solid microfibers due to nonsolvent-induced phase separation. During this wet-spun process, once the solid microfibers were wound on the rotate mandrel, an additional pulling force will act on the solid microfibers, which led to decreased diameter of formed microfibers (Table 2). On the other hand, with increasing rotation speed, the speed of winding

solid microfibers would increase, resulting in the fusion between microfibers due to the residual solvent ( $\text{CHCl}_3$  and THF) in microfibers. As a result, the scaffold structure becomes more compact and thus the porosity is decreased. We did not measure pore size because of the irregular pore structure.

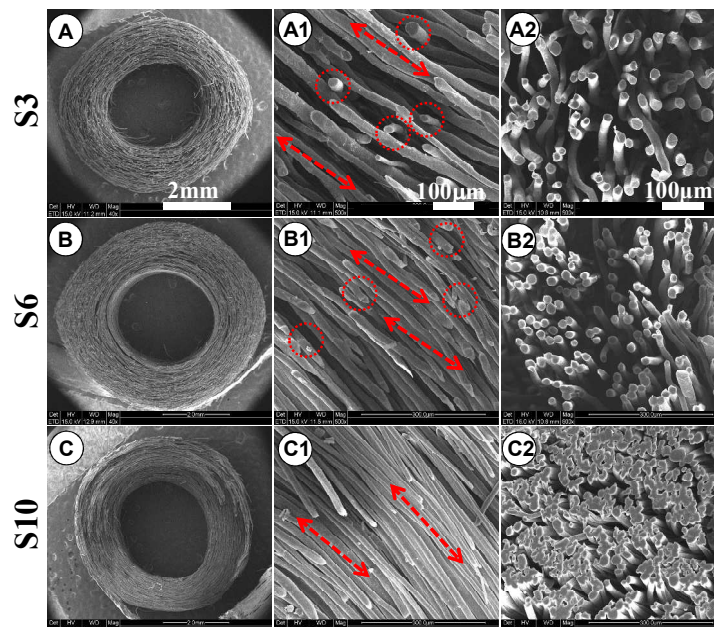


**Fig. 4** Scanning electron microscopy (SEM) images of the 3D scaffolds prepared by collecting poly ( $\epsilon$ -caprolactone) (PCL) microfibers onto a mandrel at rotating speed of 300 (A, A1, A2), 600 (B, B1, B2) and 1000 rpm (C, C1, C2). Gross morphologies of 3D scaffolds (A, B, C). High-magnification images of cross-sections (A1, B1, C1) and longitudinal sections (A2, B2, C2) of 3D scaffolds. S3, S6 and S10 denote that the scaffolds prepared at 300, 600 and 1000 rpm respectively. Red double arrows indicate parallel oriented microfibers. Dotted circles indicate crossed fibers. Scale bars are 2 mm for A, B and C, 100  $\mu\text{m}$  for A1, B1 and C1, 100  $\mu\text{m}$  for A2, B2 and C2.

### 3.2 Cell behavior in 3D scaffolds

For cell-based tissue engineering, the seeded cells should easily infiltrate inside the 3D scaffold to form a cell-scaffold composite.<sup>35</sup> To meet this requirement, the scaffold needs to have appropriate porosity. Therefore, we investigated firstly the infiltration behavior of AFCs in S3, S6 and S10 scaffolds. We found that most AFCs seeded onto S3 scaffolds leaked out to the bottom of the scaffold resulting in very low cell-seeding efficiency, while the seeded AFCs were mainly limited on the top of S10 scaffolds mainly due to the low porosity (data not shown). In comparison, the AFCs could infiltrate and distribute throughout the S6 scaffold, so we chose the S6 as

scaffold to carry out the next experiments.

From SEM results, the seeded AFCs could attach onto the surface of fibers and spread along the axial direction of the PCL microfibers (Fig. 5A2). After 14 days, cells covered the entire surface of the PCL scaffold with ECMs deposition (Fig. 5A4). Phalloidin and DAPI staining for actin cytoskeleton (red) and cell nuclei (blue) showed that the AFCs spread out and mostly stretched along the oriented microfibers (Fig. 5B). Live/dead staining of cell-scaffold constructs after 14 days' culture showed that AFCs could survive well long-term in the scaffolds as indicated by green fluorescence and no red fluorescence (Fig. 5C). Fluorescent images from longitudinal sections of cell-scaffold samples showed that DiI-labeled AFCs could penetrate into the scaffold and throughout the whole scaffolds after 14 days culture (Fig. 5D).

Shao et al developed an alginate/chitosan hybrid fiber scaffold by wet-spinning method.<sup>36</sup> The resulted scaffold had a loose structure with poor 3D integrity. The alginate/chitosan hybrid fibers exhibit irregular ribbon-like morphology with diameter varying between 40-100  $\mu\text{m}$  which can't guide oriented growth of AFCs and oriented deposition of AF-related ECMs. By contrast, our experimental results illustrated that the wet-spun PCL scaffolds exhibited a good cellular compatibility for AFCs. Furthermore, the PCL microfibers with diameter up to about 15  $\mu\text{m}$  could not only guide the AFCs orientation but also simultaneously allow AFCs to penetrate inside scaffolds. This finding may provide a new method for fabricating 3D fibrous scaffolds for tissue engineering of AF.

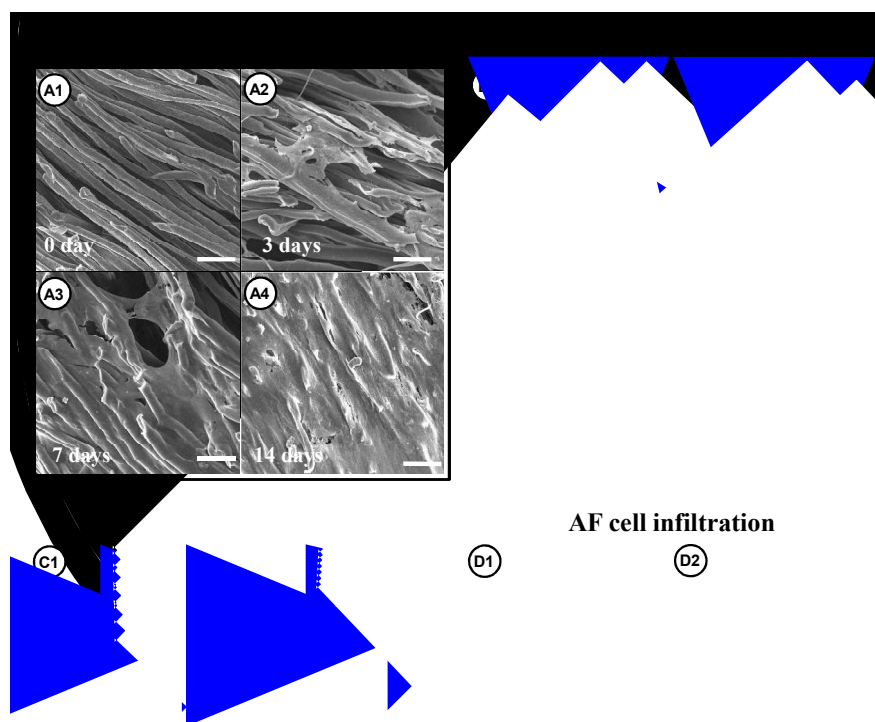


**Fig. 5** Cell behavior in 3D scaffolds. (A) SEM of AF cell attachment after 3, 7 and 14 days of culture. (B) Confocal microscopy of AF cell morphology with phalloidin and DAPI staining, (B1, B3) fluorescence images of AFCs after culture for 7 (B1) and 14 (B3) days, (B2, B4) Merged fluorescence images of AFCs and optical images of microfibers after culture for 7 (B2) and 14 (B4) days; white arrows indicate AFCs oriented along the direction of the microfibers. (C1) Confocal microscopy of live/dead stained AFCs on the scaffold after 14 days' culture; (C2) merged images of fluorescence of live/dead staining and optical images of microfibers. (D) Cross-sections of scaffolds showing distribution and morphology of DiI-labeled AFCs in scaffolds after 7 (D1) and 14 days (D2) of culture. Corresponding insets are longitudinal sections of the scaffold indicating that AFCs could penetrate the scaffold.

### 3.3 AFCs metabolic activity and ability to secrete ECM

To evaluate the metabolic activity of seeded AFCs in the scaffold, we conducted MTT assay and DNA quantification (Fig. 6). We observed that the OD value of MTT assay significantly increased from day 1 to day 21 ( $p < 0.01$ ) (Fig. 6A), indicating that the scaffold had no significant cytotoxic effects and could support cell proliferation. This finding was further confirmed by increased DNA content (Fig. 6B). Additionally, the ability of AFCs in scaffolds to secrete ECM was evaluated by quantitative biochemical analysis (Fig. 6C). We found that GAGs and collagen content increased

with culture time, where the content of GAGs increased sharply from  $3.53 \pm 1.03$  to  $28.57 \pm 3.52$  ng/scaffold(mg). The content of collagen type I, one of the major collagen components of AF tissue, was higher than collagen type II content (Fig. 6D).

To directly observe the distribution and orientation of AFCs and AF-related ECMs inside scaffolds, we performed histological and immunohistochemical staining after 7 and 21 days of culture. We found that AFCs appeared to be oriented (Fig. 7A and B), which was further revealed by DAPI staining with elongated cell nuclei (Fig. 7C and D). Safranin-O positive staining showed that AFCs produced oriented GAGs, which increased with culture time (Fig. 7E and F). Immunohistochemical staining showed that the intensity of positive staining for both collagen types I and II was stronger at 21 than at 7 days. Moreover, the intensity of staining for collagen type I was stronger than collagen type II staining at the same time of culture. The excreted GAGs and collagen showed an oriented manner with strong structural organization (Fig. 7E-J). Based on the above results, we supposed that the oriented scaffold architecture could maintain the AF cell metabolic activity and support AFCs to secrete AF-related ECMs along the direction of microfibers. This organized AF-related ECMs inside scaffold resembled that of native AF tissue.

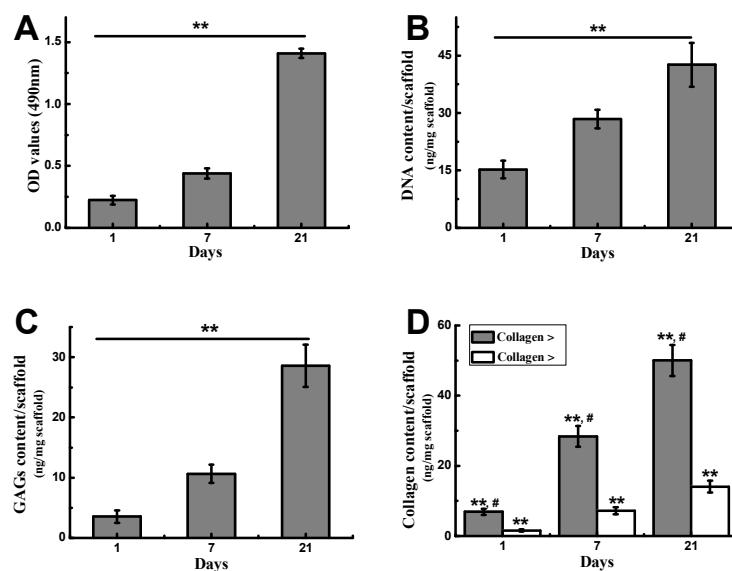


**Fig. 6** AF cell metabolic activity (A) on the scaffold, and biochemical analysis of (B) DNA, (C) glycosaminoglycans (GAGs), (D) collagen type I and II after 1 to 21 days of culture. Data are mean $\pm$ SD ( $n=3$ ). \*\*  $p<0.01$  indicate significant difference for the same sample at different culture days. #  $p<0.01$  indicate significant difference between collagen type I and II on the same culture day.

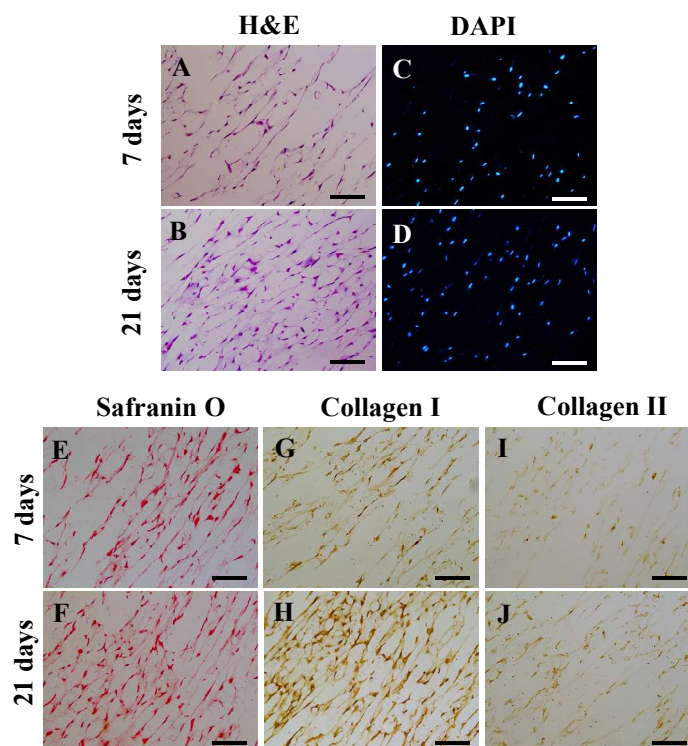


**Fig. 7** Histological and immunohistochemical analysis. (A, B) H&E staining for AFCs inside scaffold. (C, D) DAPI staining for cell nuclei (E, F) Safranin-O staining for GAGs. Immunohistochemical staining for (G, H) collagen type I and (I, J) collagen type II.

### 3.4 Real-time PCR analysis of expression of AFC phenotype-related genes

To further support the results from histological observation and biochemical analysis, the expression of AFC phenotype-related genes (*aggrecan*, *Col 1a1* and *Col 11a1*) were evaluated (Fig. 8). The expression of *aggrecan*, *Col 1a1* and *Col 11a1* was significantly up-regulated with culture time. The expression of both *Col 1a1* and *aggrecan* was up-regulated to about 2.5-fold higher at 21 days than at 1 day ( $p < 0.01$ ), which was higher than that of *Col 11a1* up-regulation of less than 1.5-fold. These results agreed well with biochemical data (Fig. 6) and histological observation (Fig. 7), suggesting that 3D oriented-PCL scaffolds could maintain an AF phenotype and support AF tissue-specific features.

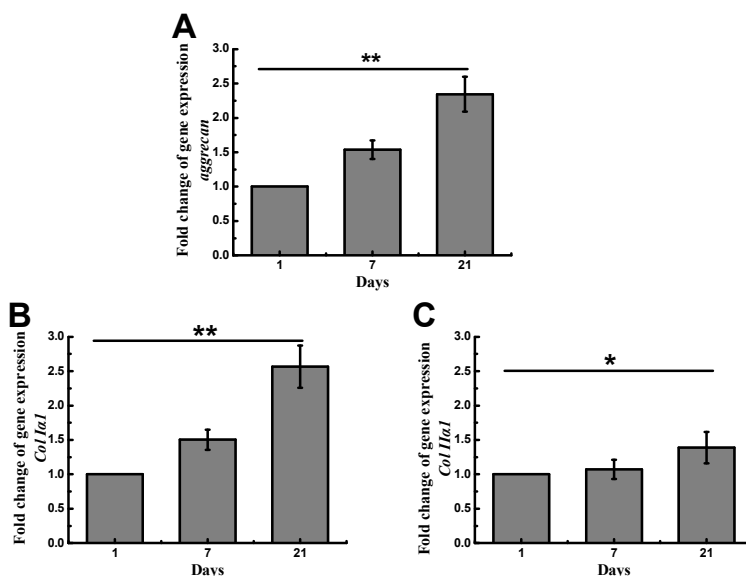


**Fig. 8** Expression of AF-cell phenotype-related genes (A) *aggrecan*, (B) collagen type I $\alpha$ 1 (*Col Iα1*), and (C) collagen type II $\alpha$ 1 (*Col IIα1*) after 7 and 21 days of culture. \*  $p < 0.05$ , \*\*  $p < 0.01$ .

### 3.5 Biomechanical properties of engineered AF constructs

Besides good biocompatibility, mechanical property is also an important parameter for AF scaffolds.<sup>36-38</sup> In the current study, both compressive modulus and tensile modulus increased with culture time (Fig. 9). Compressive modulus after 21 days of culture reached  $0.26 \pm 0.03$  MPa, which was significantly higher than  $0.17 \pm 0.02$  MPa of blank scaffold ( $p < 0.01$ ) (Fig. 9A). Tensile modulus increased to  $11.23 \pm 1.89$  MPa after 21 days of culture from  $10.03 \pm 1.37$  MPa of blank scaffold (Fig. 9B), however, the difference was not statistically significant which might be due to relative short culture period. It was expected that the tensile modulus would be enhanced with culture time.<sup>19,22</sup> These results indicate that the fabricated AF scaffolds have suitable mechanical properties that meet the requirement for AF tissue engineering.<sup>12,19</sup>

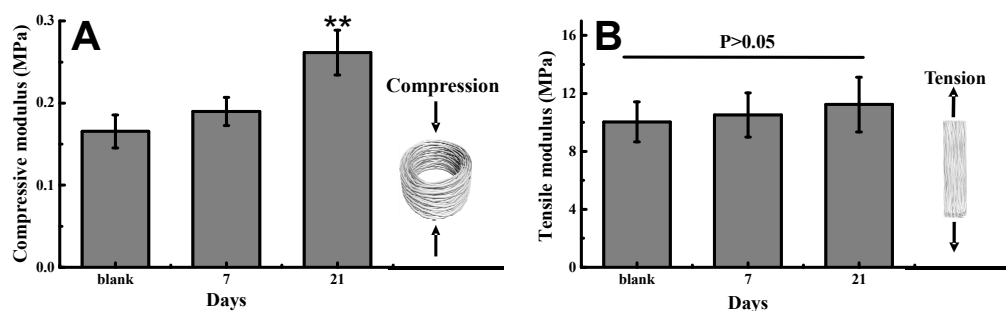


**Fig. 9** Mechanical testing of fabricated scaffolds. (A) Compressive modulus and (B)

tensile modulus of scaffold seeded with AFCs after 7 and 21 days' culture. Data are mean  $\pm$ SD ( $n=3$ ). \* $p<0.05$ , \*\* $p<0.01$ .

In the current work, we successfully fabricated a circumferentially oriented PCL microfibers 3D scaffold by wet-spinning and demonstrated its potential feasibility for application in AF tissue engineering. However, several issues remain to be further studied: ① Because there are different types of cells and biochemical composition between the inner layer and the outer AF layer.<sup>39-41</sup> Therefore, engineering the inner layer and the outer AF layer with different types of cells and biochemical composition is attracting need to be considered.<sup>42</sup> ②The cellular behaviors of other cell types including chondrocytes and stem cells need to be further evaluated. ③The ability of this kind of scaffold to integrate with adjacent vertebrae needs to be tested *in vivo*. Despite these limitations, this study provides a rational alternative to damaged AF tissue.

#### 4. Conclusions

In summary, a new circumferentially oriented PCL microfiber 3D scaffold mimicking the native AF was successfully fabricated by wet-spinning. The fabricated scaffold could support AF cell attachment, proliferation and infiltration. More importantly, this scaffold could guide oriented growth of AFCs and oriented deposition of AF-related ECMs (collagen type I, II and GAGs), which enhanced the mechanical properties. Our developed wet-spinning process holds great potential for tissue engineering of AF and other structural anisotropy conditions typical of tissues such as tendons, ligaments and the knee meniscus.

#### Acknowledgments

This study was supported by the National Natural Science Foundation of China (31300798, 81272046 and 31470937), National Program on Key Basic Research Project (973 Program, 2011CB606202), and Program for Changjiang Scholars and Innovative Research Team in University (IRT13023). The Research Foundation of the Tianjin Health Bureau (No. 14KG121).

#### References

- 1 Y. Sun, M. Hurtig, R. M. Pilliar, M. Gryn timer and R. A. Kandel, *J. Orth. Res.*, 2001, **19**, 1078-1084.

- 2 K. Broberg, *Spine*, 1983, **8**, 151-165.
- 3 M. Humzah and R. Soames, *The Anatomical Record*, 1988, **220**, 337-356.
- 4 M. A. Adams and P. J. Roughley, *Spine*, 2006, **31**, 2151-2161.
- 5 J. Urban and S. Roberts, *Arthritis Res.*, 2003, **5**, 120-138.
- 6 P. A. Anderson and J. P. Rouleau, *Spine*, 2004, **29**, 2779-2786.
- 7 R. J. Hoogendoorn, M. N. Helder, P. I. Wuisman, R. A. Bank, V. E. Everts and T. H. Smit, *Spine*, 2008, **33**, 1337-1343.
- 8 R. D. Bowles, H. H. Gebhard, R. Härtl and L. J. Bonassar, *Proceedings of the National Academy of Sciences*, 2011, **108**, 13106-13111.
- 9 S. van Uden, J. Silva-Correia, V. Correlo, J. Oliveira and R. Reis, *Biofabrication*, 2015, **7**, 015008.
- 10 B. R. Whatley, J. Kuo, C. Shuai, B. J. Damon and X. Wen, *Biofabrication*, 2011, **3**, 015004.
- 11 Y.-C. Huang, J. P. Urban and K. D. Luk, *Nature Reviews Rheumatology*, 2014, **10**, 561-566.
- 12 B. R. Whatley and X. Wen, *Mat. Sci. Eng. C*, 2012, **32**, 61-77.
- 13 D. M. O'Halloran and A. S. Pandit, *Tissue Eng.*, 2007, **13**, 1927-1954.
- 14 F. Marchand and A. M. Ahmed, *Spine*, 1990, **15**, 402-410.
- 15 J. Cassidy, A. Hiltner and E. Baer, *Connect. Tissue Res.*, 1989, **23**, 75-88.
- 16 S. H. Park, E. S. Gil, B. B. Mandal, H. Cho, J. A. Kluge, B. H. Min and D. L. Kaplan, *J. Tissue Eng. Regen. Med.*, 2012, **6**, s24-s33.
- 17 N. L. Nerurkar, D. M. Elliott and R. L. Mauck, *J. Orth. Res.*, 2007, **25**, 1018-1028.
- 18 L. Koepsell, T. Remund, J. Bao, D. Neufeld, H. Fong and Y. Deng, *J. Biomed. Mater. Res. A*, 2011, **99**, 564-575.
- 19 N. L. Nerurkar, D. M. Elliott and R. L. Mauck, *J. Biomech.*, 2010, **43**, 1017-1030.
- 20 R. L. Mauck, B. M. Baker, N. L. Nerurkar, J. A. Burdick, W.-J. Li, R. S. Tuan and D. M. Elliott, *Tissue Eng. Reviews*, 2009, **15**, 171-193.
- 21 N. L. Nerurkar, S. Sen, A. H. Huang, D. M. Elliott and R. L. Mauck, *Spine*, 2010, **35**, 867-873.
- 22 N. L. Nerurkar, B. M. Baker, S. Sen, E. E. Wible, D. M. Elliott and R. L. Mauck, *Nat. Mater.*, 2009, **8**, 986-992.
- 23 L. Koepsell, L. Zhang, D. Neufeld, H. Fong and Y. Deng, *Macromol. Biosci.*, 2011,

- 11**, 391-399.
- 24 N. Wismer, S. Grad, G. Fortunato, S. J. Ferguson, M. Alini and D. Eglin, *Tissue Eng. Part A*, 2014, **20**, 672-682.
- 25 R. Kang, D. Q. S. Le, H. Li, H. Lysdahl, M. Chen, F. Besenbacher and C. Bünger, *J. Mater. Chem. B* 2013, **1**, 5462-5468.
- 26 D. M. Lavin, M. W. Harrison, L. Y. Tee, K. A. Wei and E. Mathiowitz, *J. Biomed. Mater. Res. A*, 2012, **100**, 2793-2802.
- 27 E. Mathiowitz, D. M. Lavin and R. A. Hopkins, *Ther. Deliv.*, 2013, **4**, 1075-1077.
- 28 S. H. Park, T. G. Kim, H. C. Kim, D.-Y. Yang and T. G. Park, *Acta Biomater.*, 2008, **4**, 1198-1207.
- 29 A. Tamayol, M. Akbari, N. Annabi, A. Paul, A. Khademhosseini and D. Juncker, *Biotechnol. Adv.*, 2013, **31**, 669-687.
- 30 C. P. Barnes, S. A. Sell, E. D. Boland, D.G. Simpson, G. L. Bowlin, *Adv. Drug Deliv. Rev.* 2007, **59**, 1413-1433
- 31 K. Wang, M. Xu, M. Zhu, H. Su, H. Wang, D. Kong and L. Wang, *J. Biomed. Mater. Res. A.*, 2013, **101**, 3474-3481.
- 32 Y.-J. Kim, R. L. Sah, J.-Y. H. Doong and A. J. Grodzinsky, *Anal. Biochem.*, 1988, **174**, 168-176.
- 33 R. W. Farndale, C. A. Sayers and A. J. Barrett, *Connect. Tissue Res.*, 1982, **9**, 247-248.
- 34 B. Gossiau and H.-J. Barrach, *J. Immunol. J. Immunol. Methods*, 1979, **29**, 71-77.
- 35 R. Lanza, R. Langer and J. P. Vacanti, Principles of tissue engineering, *Academic press*, 2011.
- 36 X. Shao, C. J. Hunter. *J. Biomed. Mater. Res. A.*, 2007, **82(3)**: 701-710.
- 37 D. Ambard and F. Cherblanc, *Ann. Biomed. Eng.*, 2009, **37**, 2256-2265.
- 38 T. Green, M. Adams and P. Dolan, *Eur. Spine J.*, 1993, **2**, 209-214.
- 39 S. Ebara, J. C. Iatridis, L. A. Setton, R. J. Foster, V. C. Mow and M. Weidenbaum, *Spine*, 1996, **21**, 452-461.
- 40 D. Skaggs, M. Weidenbaum, A. Ratcliffe and V. Mow, *Spine*, 1994, **19**, 1310-1319.
- 41 J. Li, C. Liu, Q. Guo, H. Yang and B. Li, *PloS one*, 2014, **9**, e91799.
- 42 M. Bhattacharjee, S. Chameettachal, S. Pahwa, A. R. Ray and S. Ghosh, *ACS Appl. Mater. Interfaces*, 2013, **6**, 183-193.

Table 1. Primer sequences for RT-PCR

Gene	Primer sequence	
	forward	reverse
<i>Aggrecan</i>	GCCACTGTTACCGTCACTTCC	ATTCCACTCGCCCTTCTCG
<i>Col Ia1</i>	CAATCACGCCTCTCAGAACA	TCGGCAACAAGTTCAACATC
<i>Col IIa1</i>	CAACAACCAGATCGAGAGCA	CCAGTAGTCACCGCTCTTCC
<i><math>\beta</math>-actin</i>	GCTATTTGGCGCTGGACTT	GCGGCTCGTAGCTCTTCTC

*Col Ia1*(collagen type Ia1); *Col IIa1*(collagen type IIa1).

Table 2. Diameter of fiber and porosity of scaffolds at different rotating speeds

scaffold name	Rotation speed (rpm)	Diameter of fiber ( $\mu\text{m}$ )	Porosity of scaffold (%)
S3	300	22.96 $\pm$ 4.48	81.24 $\pm$ 8.75
S6	600	16.13 $\pm$ 2.77	69.33 $\pm$ 6.67
S10	1000	11.62 $\pm$ 3.21	42.58 $\pm$ 4.39